Research Article

Alfio Torrisi*, Francesco Cappellani, Caterina Gagliano, Alfonso Spinello, Federico Visalli and Lorenzo Torrisi

# Optical and mechanical characterization of UV-irradiated hydrophobic acrylic intraocular lenses

https://doi.org/10.1515/phys-2025-0283
Received January 10, 2026; accepted March 9, 2026;
published online April 27, 2026

**Abstract:** Hydrophobic acrylic intraocular lenses (IOLs) undergo significant optical, chemical, surface, and mechanical changes upon prolonged ultraviolet (UV) exposure. We assessed a commercial hydrophobic acrylic IOL using an accelerated UV protocol (1–25 h) and a multimodal workflow combining UV–Vis spectrophotometry, ATR–FTIR spectroscopy, contact-angle measurements, and Shore C hardness testing. UV–Vis spectroscopy revealed up to a 40 % decrease in UV transmittance after 25 h, and a 36–50 % increase in absorbance extending into the short-wavelength visible region, consistent with the formation of additional absorbing centers that may influence long-term optical quality. ATR-FTIR analyses indicated photochemical modifications in the acrylate backbone compatible with photo-oxidation, including chain scission and ester rearrangement. Wettability showed a transient hydrophobic shift with peaks at approximately 3 h for both test liquids, with a more pronounced hydrophobic shift for the glucose solution, followed by a return to baseline by 25 h, suggesting competing surface reorganization and oxidation processes. Shore C hardness increased from 63.0 to 73.1 after 25 h, indicating UV-induced stiffening. To our knowledge, this is the first study to simultaneously report these four modalities together for accelerated UV aging of a single hydrophobic acrylic IOL model.

**Keywords:** hydrophobic acrylic; intraocular lenses; optical analysis; photochemical degradation; UV irradiation

## 1 Introduction

The use of intraocular lenses (IOLs) has played a crucial role in transforming cataract surgery into one of the safest and most effective procedures in modern medicine. Beyond the surgical procedure itself, visual rehabilitation after cataract extraction also relies on the physical and chemical properties of the implanted lens. Over the years, various IOL materials have been developed, each exhibiting distinct advantages and disadvantages in terms of mechanical behavior, optical performance, and interaction with ocular tissues [1]. Among these, hydrophobic acrylic polymers have become one of the primary materials chosen in routine cataract surgery, due to their superior performance in a wide range of clinical contexts [2, 3]. Hydrophobic acrylic IOLs are composed of copolymers with very low water content (typically below 1 % [4]), exhibiting high structural integrity, long-term stability, and excellent biocompatibility [5]. Their low water absorption significantly reduces the risk of surface calcification and internal opacification, complications more commonly seen in hydrophilic acrylic lenses [6, 7]. Moreover, the relatively high glass transition temperature of these polymers ensures that the lens maintains its shape and mechanical consistency at physiological temperatures, allowing reliable folding and implantation through small surgical incisions [8–10].

One of the most significant clinical advantages of hydrophobic acrylic lenses is their reduced tendency to induce posterior capsule opacification (PCO), the most common late complication following cataract surgery [11, 12]. The smooth, non-adhesive surface and sharp optic edge of

***Corresponding author: Alfio Torrisi**, Department of Medicine and Surgery, Kore University of Enna, Enna 94100, Italy,
E-mail: alfio.torrisi@unikore.it. https://orcid.org/0000-0003-2404-5062
**Francesco Cappellani and Caterina Gagliano**, Department of Medicine and Surgery, Kore University of Enna, Enna 94100, Italy; and Eye Center "G.B. Morgagni-DSV", Catania 95100, Italy.
https://orcid.org/0009-0007-6807-9455 (F. Cappellani).
https://orcid.org/0000-0001-8424-0068 (C. Gagliano)
**Alfonso Spinello**, Eye Center "G.B. Morgagni-DSV", Catania 95100, Italy
**Federico Visalli**, Department of Ophthalmology, Catania University, Catania 95123, Italy. https://orcid.org/0009-0005-6710-2460
**Lorenzo Torrisi**, MIFT Department, Messina University, Messina 98166, Italy. https://orcid.org/0000-0003-0853-136X

these lenses create a less favorable environment for the adhesion and migration of residual lens epithelial cells, which are primarily responsible for fibrotic changes on the posterior capsule [13]. As a result, patients implanted with hydrophobic acrylic IOLs require fewer Nd:YAG laser pulse ablation processes [14] (capsulotomies) and maintain better long-term visual acuity compared to those with hydrophilic lenses [15–17].

In contrast, hydrophilic acrylic lenses, typically based on hydroxyethyl methacrylate (HEMA) and with water content ranging between 18 % and 30 %, offer greater flexibility but also promote increased protein adsorption and cellular adhesion [18]. This biological behavior has been consistently linked to a higher incidence of PCO and other postoperative complications, particularly in eyes affected by systemic diseases or ocular inflammation. Surface grafting strategies based on phosphorylcholine-containing copolymers have been explored to improve uveal and capsular biocompatibility of hydrophobic acrylic IOLs [19].

Other materials, such as polymethylmethacrylate (PMMA) and silicone [20–22], are nowadays used less frequently in clinical ophthalmology. PMMA lenses, although optically stable, are rigid and require large incisions [9]. Silicone lenses, on the other hand, are foldable but are associated with increased glistening formation and are contraindicated in eyes requiring silicone oil tamponade, such as those undergoing retinal surgery [23].

Hydrophobic acrylic IOLs also offer notable resistance to glistening-microscopic water-filled vacuoles within the lens material, which can scatter light and reduce contrast sensitivity [24]. Furthermore, the ability to maintain its intended optical power and position over time, ensuring predictable and durable refractive outcomes following cataract surgery, as it was demonstrated by recent IOLs made of hydrophobic polymers is also noteworthy [25, 26].

Due to the high photon energy, higher than 3 eV, UV radiation induces polymer-chain scission, oxidation, radical formation, and cross-linking phenomena, which alter the material in proportion to the absorbed dose and penetration depth, as reported in the literature for many polymeric species [21, 27].

Thanks to these combined properties, low water uptake, high optical clarity, long-term biostability, and low complication rates, hydrophobic acrylic IOLs are now considered the benchmark against which other IOL materials are compared.

This paper explores the reasons for their widespread adoption, focusing on the material's chemical characteristics, surface behavior, and clinical performance. A comparative analysis will also highlight the specific context in which hydrophobic acrylic lenses provide clear advantages over hydrophilic and other traditional materials. Recent reviews summarize next-generation and patient-specific IOL materials and surface engineering approaches [28].

The photostability of intraocular lens materials under ultraviolet (UV) exposure has been investigated since the late 1990s, with early studies reporting yellowing, surface cracking, and polymer degradation in PMMA and first-generation acrylics. Recent investigations have focused on hydrophobic acrylates and silicone-based IOLs, examining changes in transmittance, mechanical stiffness, and surface wettability after prolonged UV irradiation.

Since intraocular lenses are long-term implants, UV-related aging processes can accumulate over years, and even relatively slow photo-oxidative mechanisms may reach clinically relevant levels when integrated over decades. *In vivo*, the UV component reaching the IOL is attenuated and spectrally filtered by the ocular media, i.e. the cornea, aqueous humor, and (prior to surgery) the crystalline lens, which together substantially reduce UV radiation before it reaches intraocular structures [29]. Therefore, the present accelerated UV protocol was adopted as a controlled stress condition to reveal and quantify polymeric changes. Accordingly, accelerated irradiation protocols such as those employed in this study should be regarded as a standardized accelerated UV irradiation study aimed at highlighting UV-driven degradation mechanisms within practical experimental timescales, without implying a direct correspondence with *in vivo* exposure time or fluence [30].

Hydrophobic acrylic IOLs are generally preferred over hydrophilic materials because of their lower water uptake, reduced tendency to calcification, lower incidence of posterior capsule opacification, and superior long-term mechanical and optical stability. Their higher glass-transition temperature and reduced protein adsorption contribute to more predictable refractive outcomes and improved biocompatibility over decades of implantation.

For example, it was already demonstrated UV-induced absorbance and FTIR modifications in PMMA lenses exposed to 365 nm light [31], as well as complementary evidence of photochemical degradation and bond scission in PMMA under similar irradiation conditions [21]. Exposure models and biomolecular changes in ocular tissues under UV stress were reviewed [32], reinforcing the clinical importance of understanding UV-driven photo-oxidative aging in the long-term stability of intraocular lenses. Experimental evidence on the causes of intraocular lens opacification was also presented [33], further highlighting the clinical importance of material stability under environmental degradation conditions. UV irradiation

effects on hydrophilic acrylic IOLs and silicone IOLs under comparable protocols have also been previously reported by our group [7, 21, 22], providing a comparative basis for the present investigation on hydrophobic acrylic materials. These studies emphasize the importance of simulating UV-driven stress to assess optical, mechanical, and interfacial stability *in vivo*.

# 2 Materials and methods

## 2.1 Lenses and materials

Hydrophobic acrylic intraocular lenses (IOLs) are mainly composed of cross-linked acrylate polymers characterized by ester-linked carbon chains, which confer optical transparency, mechanical resistance, chemical stability, and biocompatibility.

These devices are typically manufactured from cross-linked copolymers synthesized from acrylate and methacrylate monomers. Common formulations include aromatic derivatives such as phenylethyl acrylate (PEA, $C_{11}H_{12}O_2$) and phenylethyl methacrylate (PEMA, $C_{12}H_{14}O_2$), which increase the refractive index and enhance optical clarity. Additional acrylate or methacrylate units (e.g., methyl or ethyl esters) may be incorporated to modulate flexibility and mechanical performance. These polymers exhibit high optical clarity, chemical resistance, and long-term stability, especially when combined with UV-absorbing chromophores or stabilizing additives.

The specific model investigated in this study, the *SeeLENS HP Easy* (Hanita Lenses, Israel) [34], consists of a single-piece aspheric hydrophobic acrylic IOL with a 6 mm optic diameter and a central thickness of 0.9 mm (Figure 1a–e). It is composed of cross-linked acrylate copolymers incorporating UV-absorbing chromophores and minor siloxane components to adjust its mechanical behavior, as specified in the manufacturer's technical datasheet. This model was selected for its wide clinical adoption and its

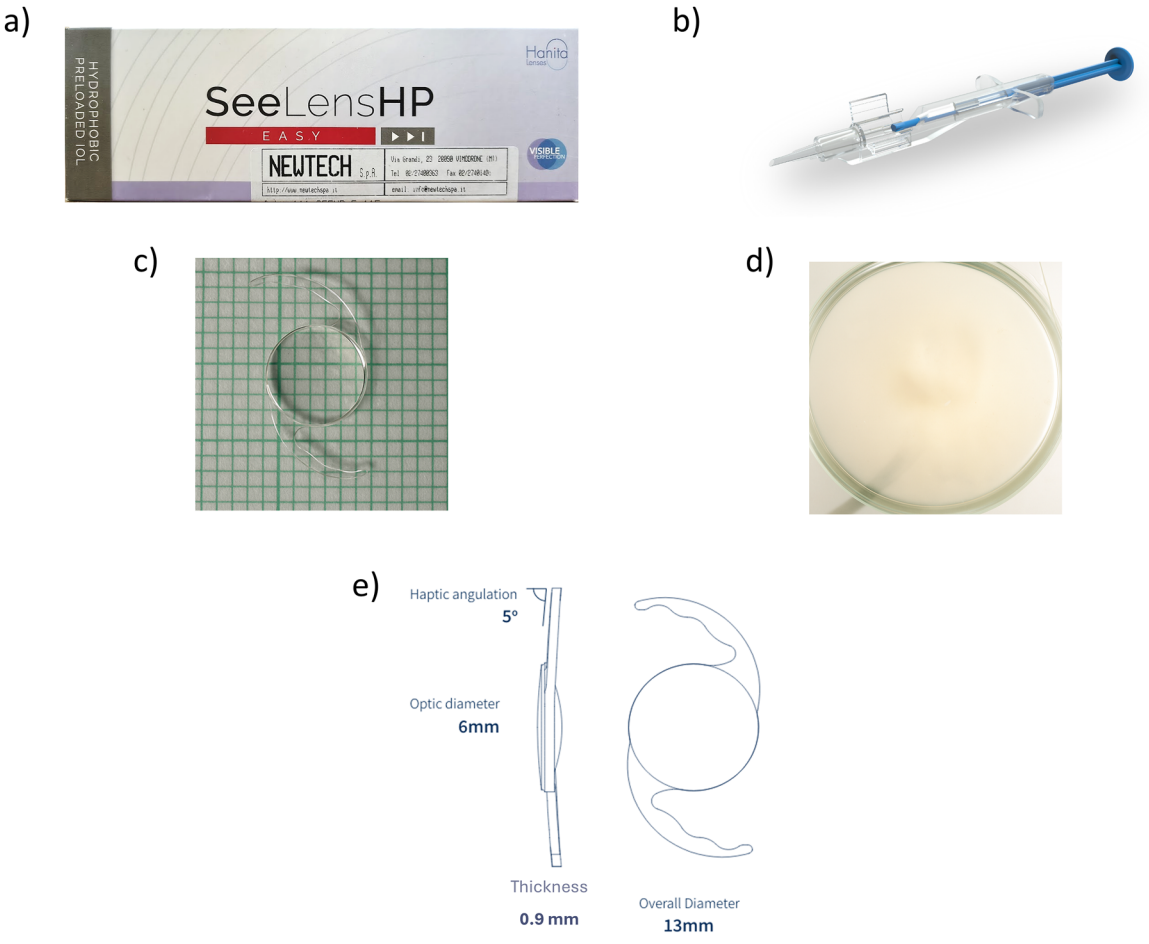


**Figure 1:** Overview of the Hanita SeeLENS HP Easy hydrophobic acrylic intraocular lens and implantation system. (a) Packaging of the Hanita – SeeLENS HP Easy hydrophobic acrylic intraocular lens. (b) Injector used for implantation. (c) Photograph of the IOL placed on millimetric paper for scale. (d) Optical micrograph of the lens surface morphology. (e) Schematic drawing of the IOL in two orthogonal views with real dimensions (optic diameter 6 mm, central thickness 0.9 mm).

representativeness of modern hydrophobic acrylic IOLs routinely used in cataract surgery.

## 2.2 UV irradiation protocol

To assess the effects of ultraviolet (UV) exposure on intraocular lenses, a set of hydrophobic acrylic IOLs was subjected in accordance with ASTM G154 standards [35]. The UV source employed was a Blak-Ray UVL-56 lamp [36] emitting at 365 nm (3.38 eV photon energy).

Two exposure conditions were defined *a priori* to represent an early and a prolonged UV-aging stage (1 h and 25 h), allowing observation of both initial and cumulative material changes. Where intermediate exposure times were required by a specific endpoint, they are reported in the corresponding methodological subsection and figure captions.

Although intraocular lenses are exposed to UV light continuously over the years, the actual fluence depends on multiple factors, including ocular anatomy, lens position, and natural filtering by the cornea and aqueous humor. IOLs are designed for long-term implantation, typically several decades. To reproduce the UV exposure within a controlled timeframe, we adopted an accelerated aging approach. The experimental conditions were held constant at all timepoints to isolate UV-driven effects in a reproducible controlled accelerated UV irradiation protocol.

Specifically, lenses were irradiated with monochromatic UV-A at 365 nm, in dry air, at room temperature (20 °C), ambient pressure (1 atm), and with a relative humidity of 45 %. Lenses were positioned at fixed lamp-to-sample distance of 3 cm, with irradiation focused on the convex anterior surface. Since UV penetration in acrylic materials is limited to approximately 100 μm, the reported effects are relevant to this superficial region.

The measured fluence at a working distance of 3 cm was ∼200 mJ/cm$^2$ and the lamp delivered a power density of 2.2 μW/cm$^2$ over 25 h irradiation.

## 2.3 UV–VIS–NIR spectrophotometry

The optical response of the IOLs was evaluated using a double-beam UV–Vis–NIR (ultraviolet–visible–near infrared) spectrophotometer (Jasco V-750, Jasco-Europe, Italy) operating in the 300–900 nm wavelength range with a 0.1 nm wavelength resolution. Spectra were corrected for atmospheric absorption. All UV–Vis measurements were acquired using double-beam normalization to eliminate spectral variations caused by lamp-intensity fluctuations. Identical irradiation conditions were maintained during all optical measurements, and the resulting spectra were normalized to the incident intensity. Each measurement was replicated across multiple lenses ($n = 5$) and subsequently averaged.

## 2.4 ATR-FTIR spectroscopy

To investigate molecular changes in the polymer matrix, ATR-FTIR spectroscopy (Attenuated Total Reflectance – Fourier Transform Infrared Spectroscopy) was employed using a Jasco 4600 FTIR spectrometer. The spectral range extended from 4,000 to 390 cm$^{-1}$, with a 4 cm$^{-1}$ wavenumber resolution, enabling the observation of UV-induced bond breaking and formation of new chemical bonds. Spectra were recorded before and after irradiation for durations from 1 h to 25 h.

## 2.5 Surface wettability

Wettability was assessed by static contact-angle measurements using the sessile-drop method. A 2 μL droplet of distilled water (DDW) or a 5 % glucose infusion solution (Glucosio Fresenius Kabi Italia; 278 mOsm/L, pH 3.5–5.5) was deposited on the IOL surface, and images were acquired at 8× magnification using a Paralux optical microscope to determine the contact angle. The glucose solution was selected as a clinically used aqueous medium and as a low-ionic-strength probe of UV-related surface-energy changes.

## 2.6 Hardness measurements

Surface hardness measurements were carried out using a portable Shore C digital durometer (GainExpress 560-10C), suitable for medium-hard polymers and elastomeric materials. Hardness was evaluated using the Shore C scale of the ASTM D2240 test, which provides a reproducible and non-destructive measure of stiffness suitable for small, curved samples such as intraocular lenses (IOLs). The Shore C scale is designed for medium-hard elastomers and plastics, overlapping with the upper range of the Shore A scale and the lower range of the Shore D scale. It offers improved precision for materials that exceed the useful range of the Shore A scale (>90 A) yet remain below the lower limit of the Shore D scale (<20 D). The indenter geometry is identical to that of Shore A (35° truncated cone), while the applied spring force corresponds to that used in the Shore D scale (44.45 N).

For this study, the Shore C scale was selected because its truncated-cone indenter, with a 0.4 mm tip diameter, is sufficiently small relative to the IOL optic (6 mm diameter, 0.9 mm central thickness) to avoid geometric constraints or interference from the haptic junction. This configuration allowed multiple localized indentations to be performed within the optic region without edge effects. Hardness

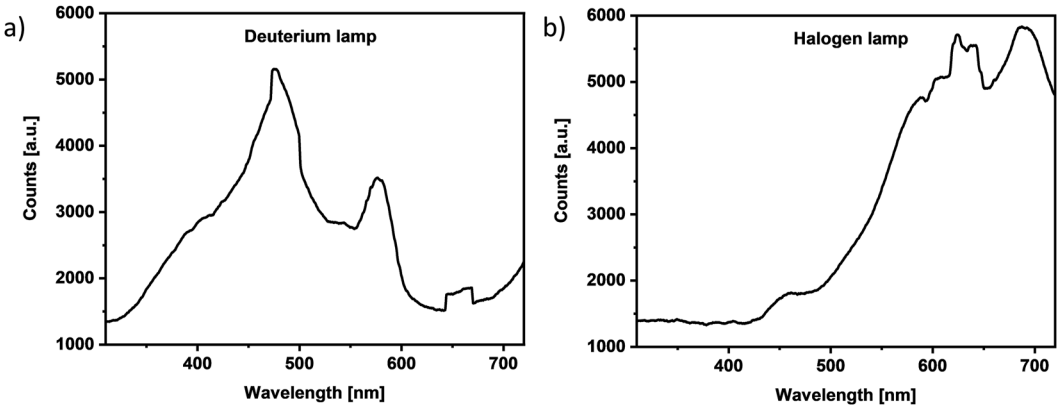


**Figure 2:** Emission spectra of the two light sources employed for optical characterization, spanning (a) the UV–Vis–NIR range for the deuterium lamp and (b) the Vis–NIR range for the halogen lamp.

measurements were therefore performed in the central optical zone, which is the area most exposed to UV irradiation. Reported values represent the mean of five measurements per sample in accordance with ASTM D2240 guidelines [37].

# 3 Results and discussion

## 3.1 Optical investigations

IOLs were irradiated with UV radiation for up to 25 h. Optical measurements were carried out using a UV–Vis–NIR spectrophotometer equipped with a deuterium lamp, spanning from 300 to 750 nm (Figure 2a), and a halogen lamp, which covers the 350–750 nm wavelength range (Figure 2b). Such spectra have been used to evaluate the absorbance and transmittance of IOL devices as a function of their damage induced by UV irradiation time.

Figure 3a and b shows the experimental data of the lens transmittance relative to the near UV–Vis region, obtained using the deuterium lamp, and the Vis-near IR region, obtained using the halogen lamp, as a function of the UV exposure time. Experimental data were collected by performing eight measurements at five different locations on each of five IOLs, and the results were subsequently averaged.

It is possible to observe that the UV irradiation time decreases the transmittance at high irradiation times, inducing some molecular damage of the polymer. Any minor early variations were within measurement variability.

The UV maximum transmittance decreases significantly, up to about 40 % after 25 h of continuous irradiation time, under a UV lamp at 365 nm, while a smaller decrease is observed in the Vis region, where it decreases to about 80–90 % for the same irradiation time. The experimental results are consistent with the rationale of

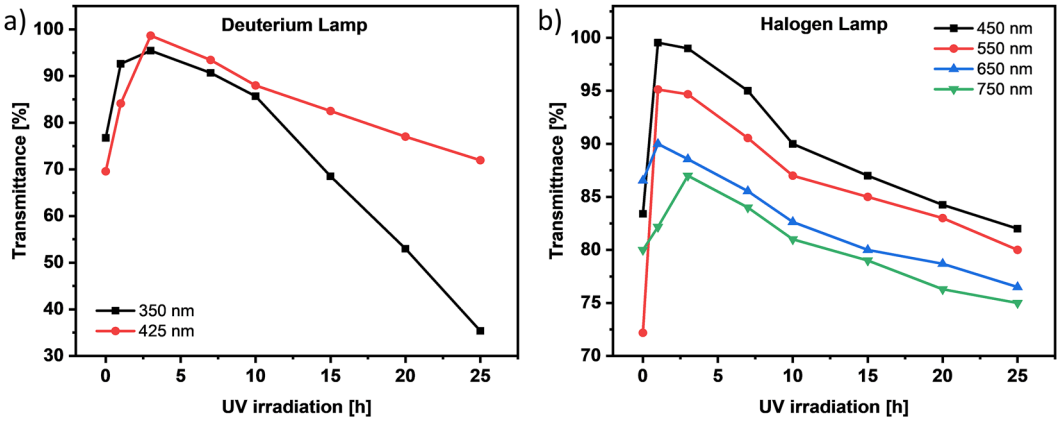


**Figure 3:** Transmittance of hydrophobic acrylic IOLs as a function of UV irradiation time at selected wavelengths, measured using (a) a deuterium lamp (300–450 nm) and (b) a halogen lamp (450–750 nm). The transmittance decreases progressively with irradiation time, particularly in the UV region and at shorter visible wavelengths.

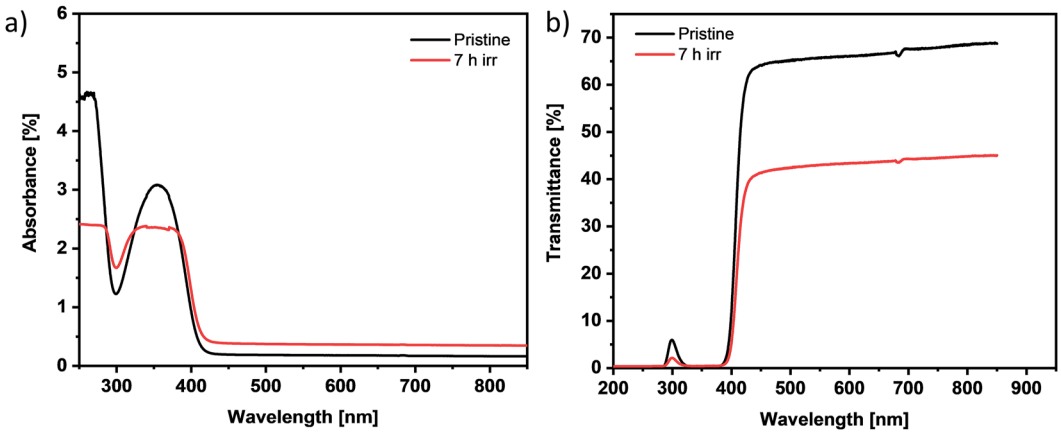


**Figure 4:** Comparison between pristine and UV-irradiated hydrophobic acrylic IOLs after 7 h of continuous UV exposure. (a) Absorbance spectra showing increased absorption in the UV region (300–400 nm) due to photochemical modifications of the acrylate matrix. (b) Corresponding transmittance spectra revealing reduced transparency across the visible range (400–700 nm). These spectral variations indicate the onset of UV-induced photo-oxidative processes.

accelerated UV photoaging protocols [30]. It is possible to note that wavelength-specific transmittance drops can exceed 50 % already after 7 h (Figure 4), reflecting the wavelength-dependent sensitivity of the material.

The observed transmittance drop suggests that UV exposure induces a progressive enhancement in the Vis absorption. Such changes may compromise the IOL's ability to remain perfectly transparent to the Vis radiation, particularly under exposure conditions, most likely due to photodegradation processes affecting the UV-absorbing chromophore components. In acrylic and methacrylic polymers, UV photons generate radicals that, particularly in the presence of oxygen, evolve toward carbonyl-containing and conjugated species, increasing absorbance in the near-UV and extending it toward the short-wavelength visible region. These newly formed absorbing centers are responsible for the progressive loss of UV and short-wavelength visible transmittance observed in Figures 3 and 4.

UV–Vis spectrophotometric analyses in both absorbance and transmittance modes were performed to evaluate the optical alterations induced by UV irradiation. Figure 4a and b shows a comparison between the spectrum of the absorbance and transmittance of a pristine IOL and that of a sample exposed to UV radiation for 7 h, respectively. The irradiation time of 7 h was selected as an intermediate condition, allowing the comparison of absorbance and transmittance spectra at a stage where UV-induced modifications are already evident but not yet extreme, thus representing a transitional profile in the accelerated aging process.

The experimental results from the transmittance spectra reveal a significant reduction, after the UV exposure, at approximately 300 nm, where transmittance decreases by around 50 % compared to the unexposed IOL. Similarly, in the UV-A region at about 400 nm, a transmittance drop of about 64 % is observed.

Correspondingly, the absorbance spectra indicate that after UV exposure, there is an increase in the average absorbance of approximately 36 % in the Vis region, while in the UV range, the average absorbance increases by approximately 50 %, consistent with the formation of new absorbing chromophores.

The observed spectral changes are consistent with photochemical and photo-oxidative processes occurring within the polymer matrix of the IOLs, leading to the formation of new absorbing centers or chromophores. The observed increase in absorbance and concurrent drop in transmittance, particularly in the UV and short-wavelength Vis range, point toward photoinduced structural modifications, such as polymer cross-linking, chain scission, or the formation of conjugated systems.

The emission intensity of deuterium and halogen sources is not uniform across wavelengths; however, this effect was compensated through double-beam correction. Observed differences therefore originate from UV-induced material modifications rather than instrumental variability.

From a functional performance perspective, although the increased UV absorption might initially seem advantageous, these changes indicate underlying material degradation, which could compromise the lens's long-term optical clarity and structural integrity. Moreover, the rise in absorbance within the Vis range may lead to distorted color perception, decreased contrast sensitivity, and diminished visual quality for the patient. Reduced short-wavelength

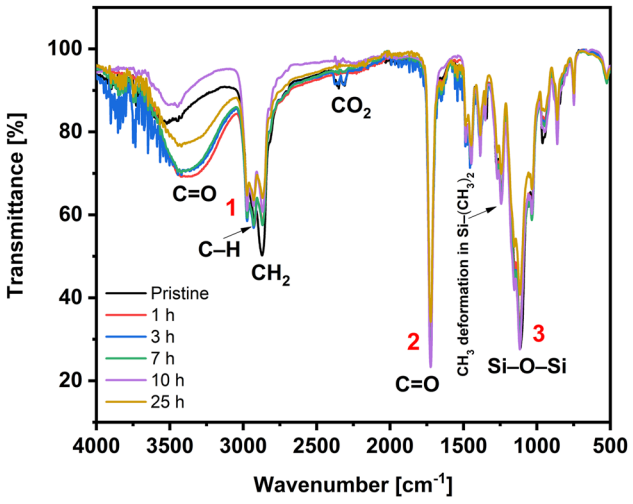


**Figure 5:** ATR–FTIR spectra of hydrophobic acrylic IOLs before and after UV irradiation (1–25 h). Changes in aliphatic C–H stretching, carbonyl vibrations, and Si–O–Si bands indicate photochemical degradation of the acrylate backbone, whereas siloxane-related bands exhibit only minor variations.

transmission may affect color perception and contrast sensitivity. Although long-term clinical studies on acrylic IOLs have not always demonstrated a statistically significant correlation between IOL surface degradation and measurable visual performance [38], dedicated follow-up assessments, including forward scatter, are warranted to quantify how UV-driven spectral changes translate into clinically relevant image quality metrics.

## 3.2 FT-IR spectroscopy

Fourier-transform infrared (FTIR) spectroscopy has been performed in the spectral range of 4,000–500 $cm^{-1}$ to assess chemical modifications occurring in hydrophobic acrylic intraocular lenses (IOLs) upon ultraviolet (UV) irradiation. Figure 5 shows a comparison of different FTIR spectra as a function of the IOL UV irradiation time, from the pristine lens up to 25 h of irradiation time. The selected time-points were chosen to represent the main stages of UV-induced evolution, initial response, intermediate transition, and final stabilization.

To better visualize the full spectrum, the spectra in Figure 5 were divided into three regions, 1, 2, and 3, as shown in detail in Figure 6a–c.

In the pristine condition, the spectrum shows well-defined absorption bands, including the C–H stretching vibrations at 2,924 $cm^{-1}$ and 2,875 $cm^{-1}$, associated with the methylene ($–CH_2$) groups from the hydrophobic acrylate monomers such as butyl acrylate (BA), 2-ethylhexyl acrylate (EHA), and decyl acrylate (DA). These features fall within Region 1 (Figure 6a), which encompasses the aliphatic moieties of the polymer matrix [18]. Moreover, in the overall FTIR spectra of Figure 5 a weak band corresponding to absorbed $CO_2$ is visible around 2,340 $cm^{-1}$ [21].

In Figure 6b (Region 2), the absorption band at 1,711 $cm^{-1}$ corresponds to the stretching vibration of the carbonyl (C=O) groups, characteristic of the ester functionalities in the acrylate backbone. A weaker overtone is also observable around 3,444 $cm^{-1}$ [39].

The broad band between 1,000 and 1,120 $cm^{-1}$, shown in Region 3 (Figure 6c) is attributed to the asymmetric stretching vibrations of Si–O–Si bonds, while the sharp signal at 1,250 $cm^{-1}$ is assigned to the deformation of methyl groups in $Si–(CH_3)_2$ group [40].

Upon UV exposure, in Region 1, a gradual increment in the transmittance occurs, i.e., a reduction in absorption intensity is detected with increasing the UV irradiation time, suggesting a partial loss of aliphatic content, likely due to photodegradation mechanisms involving chain scission or oxidative cleavage of side groups.

In Region 2, indeed, the C=O stretching band shows transmittance decreasing, i.e., absorption enhancement with the UV irradiation time, indicating possible rearrangements or cleavage of ester linkages induced by photochemical reactions.

Finally, in Region 3, the Si–O–Si stretching vibrations decrease with the UV irradiation time, enhancing the transmittance, although minor intensity fluctuations may reflect superficial reorganization or migration phenomena involving organosilicon species. This is consistent with a reduction of IR-active absorbing groups and/or changes in optical density, rather than an improvement in material integrity. The observed spectral variations confirm that UV exposure induces molecular alterations in the polymer matrix, mainly involving the acrylate phase, while the siloxane-based components exhibit higher resistance to photo-induced changes. These chemical transformations are consistent with the optical variations observed in UV–Vis analyses, supporting the occurrence of structural reconfigurations within the material.

As can be observed, for UV irradiation times exceeding 10 h, the UV transmittance of the tested hydrophobic acrylic IOLs becomes lower than that of the pristine IOL. Visible transmittance also decreases with increasing UV irradiation time. In the IR range, an apparent increase in transmittance (i.e., reduced IR absorbance) may reflect attenuation of peaks assigned to C–H and $CH_2$ vibrations and to Si–O–Si and $Si–(CH_3)_2$-related modes, and/or changes in optical density within the probed region. This trend does

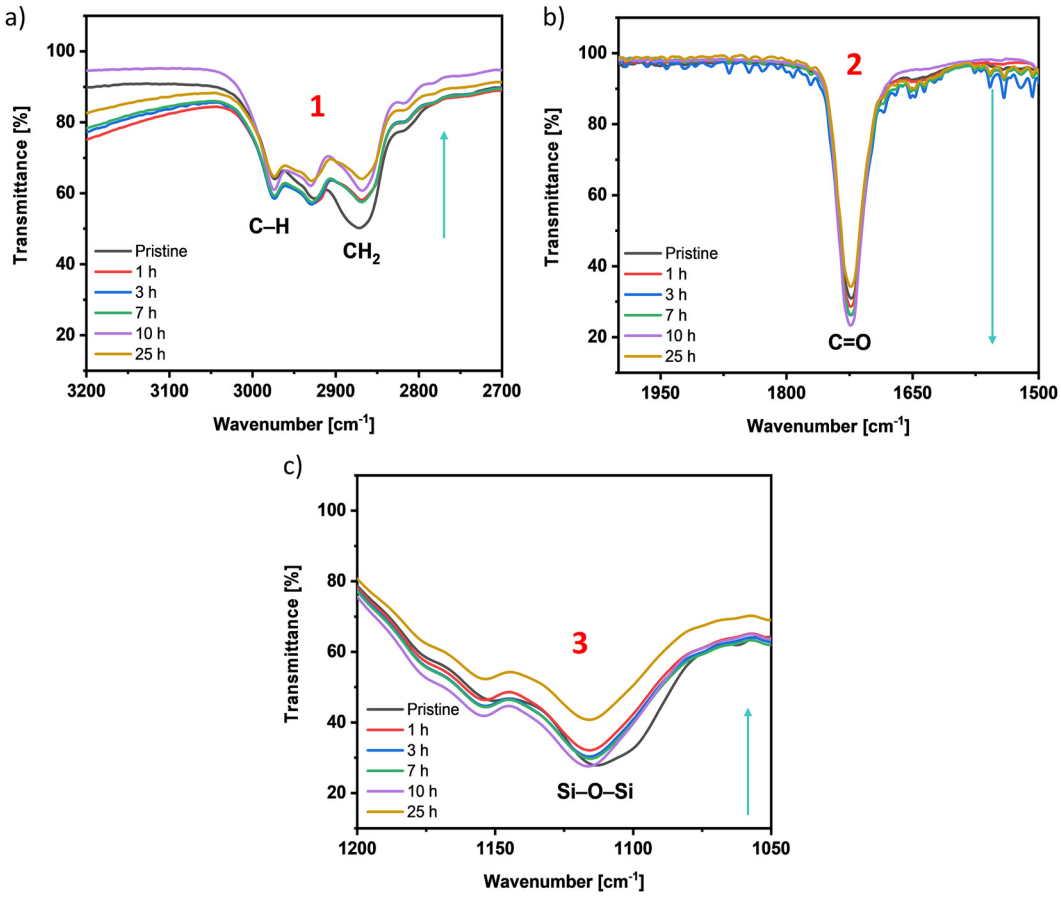


**Figure 6:** Detailed FTIR regions highlighting UV-induced molecular modifications. (a) Region 1 (3,200–2,700 $cm^{-1}$): progressive decrease in the intensity of the aliphatic C–H stretching bands at 2,924 and 2,875 $cm^{-1}$ with increasing UV exposure. (b) Region 2 (2,000–1,500 $cm^{-1}$): increased absorption in the carbonyl stretching band (C=O, ~1,711 $cm^{-1}$), indicating ester-group rearrangements. (c) Region 3 (1,200–1,050 $cm^{-1}$): reduction of Si–O–Si and Si–$(CH_3)_2$ vibrational bands, suggesting partial reorganization of siloxane structures. These spectral variations confirm UV-induced degradation and structural modifications within the acrylate matrix.

not imply improved material integrity and occurs alongside FTIR evidence of ongoing photochemical degradation, such as the progressive reduction of C–H stretching bands and subtle shifts in the carbonyl region. The progressive increase in C=O absorption and concurrent attenuation of C–H bands are consistent with oxidation and chain scission processes in the acrylate backbone that generate the new chromophoric species responsible for the increased UV–Vis absorbance reported in Section 3.1. This cross-consistency between FTIR and UV–Vis data provides mutually reinforcing evidence of photo-oxidative degradation at both the molecular and optical level.

Overall, these results indicate that molecular-level degradation does not necessarily translate into a linear trend in broadband transmittance and highlight the need to interpret optical changes together with band-specific FTIR signatures. The obtained results align with previously reported photo-oxidative behaviors in polymeric materials. Our irradiation durations of 1 h and 25 h correspond to early and cumulative exposure phases consistent with accelerated aging models applied in the literature [35].

## 3.3 Wettability measurements

The wetting angle of the solutions with the hydrophobic acrylic IOL surface is strongly dependent on the water content of the resin, temperature, and air conditions (pressure, humidity, air flux, etc.). Wettability measurements revealed a time-dependent variation in the contact angle between the liquid droplet and the IOL surface during UV irradiation. Specifically, the contact angle increased progressively during the initial exposure phase, reaching a maximum at approximately 3 h for both test liquids, with a more pronounced hydrophobic shift for the glucose solution (84°) than for distilled water (71°). The DDW curve shows a broad plateau between 3 h and 7 h before gradually returning

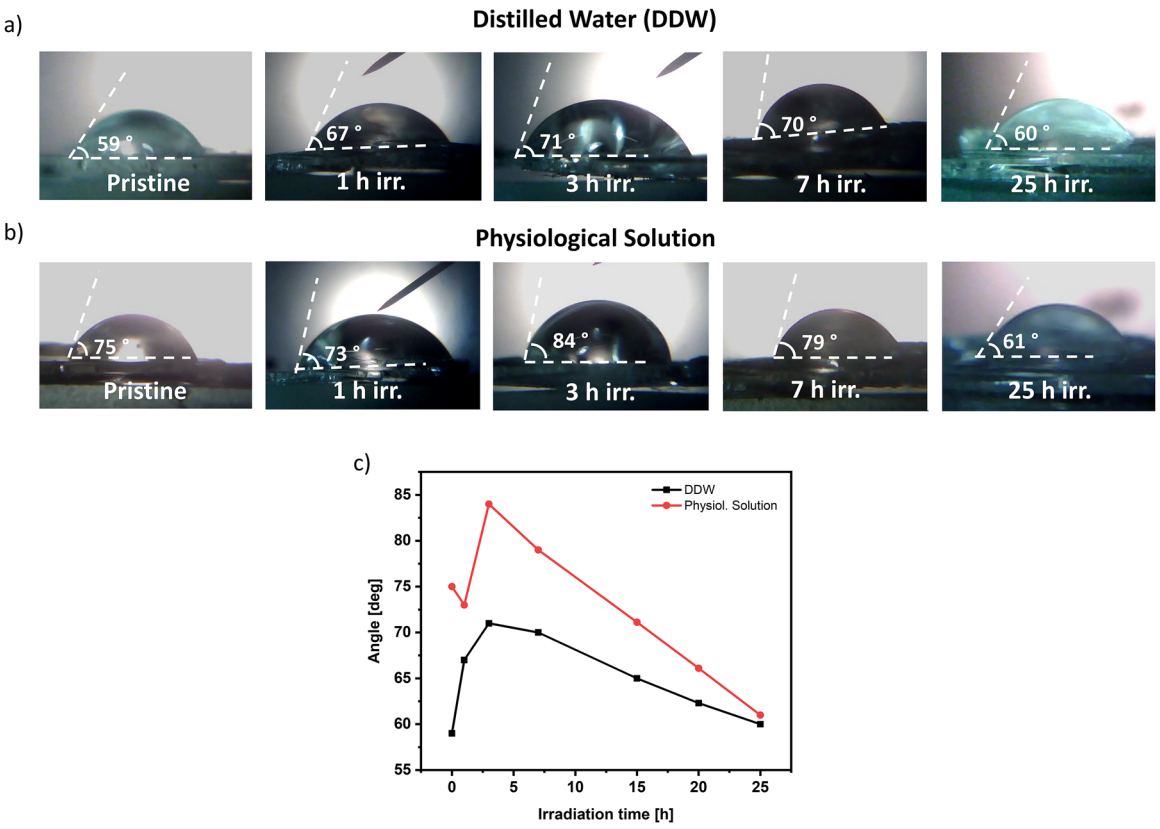


**Figure 7:** Contact-angle variation as a function of UV irradiation. (a) Distilled water droplets. (b) Infusion 5 % glucose solution droplets. (c) Contact-angle evolution over time. The maximum occurs at ∼3 h for both test liquids, followed by a gradual return to baseline at 25 h, indicating transient surface hydrophobicity.

toward baseline, whereas the glucose solution exhibits a sharper peak followed by a gradual decrease. This increase in contact angles indicates a temporary enhancement of surface hydrophobicity, likely due to UV-induced surface activation or rearrangement of polar groups. However, beyond these timepoints, the contact angle gradually decreased, ultimately returning to values comparable to the pristine condition after 25 h of irradiation. This reversible trend suggests a dynamic surface modification process, possibly involving competing mechanisms such as photo-oxidation, reorientation of surface chains, or partial recovery of the initial hydrophobic surface state. During initial UV exposure, near-surface chain scission and changes in segmental mobility promote the reorientation of nonpolar chain segments toward the polymer–air interface, temporarily reducing surface energy and increasing the contact angle. As UV exposure continues, photo-oxidation introduces polar functional groups at the surface, including hydroperoxides and carbonyl species, gradually reversing the initial hydrophobic shift. This type of peak-and-recovery behavior is consistent with competing surface reorganization and oxidation processes reported for UV-irradiated polymer surfaces more broadly [41, 42].

It is also worth observing that UV penetration into acrylic materials is confined to a limited surface layer; once this superficial region is entirely photo-oxidized and all available reactive sites have been consumed, the wettability response is expected to reach saturation. This is consistent with the contact-angle recovery toward baseline at 25 h, where photo-oxidation appears to have approached saturation. Figure 7a and b shows photographs of droplets on the IOL surface using distilled water and glucose solution, respectively, while Figure 7c reports the contact-angle evolution as a function of UV irradiation time.

Each contact-angle value represents the mean of triplicate measurements taken at five positions on each lens. The transient increase in contact angle indicates a temporary increase in surface hydrophobicity due to UV-induced rearrangement of polar groups, followed by partial recovery after extended exposure.

**Table 1:** Hardness values of the tested IOL materials. Experimental measurements were performed on the Shore C scale and compared with representative literature ranges reported on material-specific Shore scales (A or D). Differences reflect the scale dependence of durometer readings and the influence of formulation and testing conditions.

| Material | Literature hardness (original scale) | Normalized Shore C (HC) | Experimental Shore C (HC) |
|---|---|---|---|
| Hydrophobic acrylic | Not standard | N/A | 63.0–73.1 |
| PMMA | 75–85 Shore D | ∼85–90 | 70.37 |
| Hydrophilic acrylic | 47.5–57.5 Shore A | ∼10–20 | 83.56 |
| Silicone | 20–90 Shore A | ∼10–50 | 84.12 |

## 3.4 Hardness measurements (Shore C)

The hydrophobic acrylic IOLs in their pristine condition exhibited a Shore C hardness of 63.0 HC, which increased to 73.1 HC after 25 h of UV irradiation. This ∼10-point increase is a direct indicator of UV-induced structural changes, primarily cross-linking, which make the polymer more rigid and represent a well-documented phenomenon in polymer science [43]. When compared to other IOL materials, the UV-aged hydrophobic acrylic samples approached the PMMA hardness measured in this study (70.37 HC), although they remained softer than the hydrophilic acrylic (83.56 HC) and silicone (84.12 HC) measured in the same study The specific Shore C scale was chosen for its applicability to the intermediate hardness range of hydrophobic acrylics, which are widely used in IOLs due to their mechanical balance and handling requirements, and whose properties can vary with formulation [44].

The hardness increase is consistent with UV-induced modifications of the polymer matrix, such as additional cross-linking and/or surface densification, which are commonly reported in photo-aged acrylic systems. While Shore C indentation does not directly quantify bulk stiffness, it provides a sensitive screening parameter for UV-driven mechanical hardening under identical testing conditions. Prolonged UV exposure can promote photochemical reactions that alter chain packing and surface morphology, thereby contributing to the observed increase in indentation hardness.

However, direct comparison of Shore C values across materials reported on different durometer scales should be interpreted with caution. The PMMA sample, despite being typically characterized on the Shore D scale (75−85 HD [45]), yielded a value of 70.37 HC. This lower-than-expected Shore C value could be attributed to the specific PMMA formulation used, possibly including plasticizers, or to the measurement method employed. Similarly, the hydrophilic acrylic and silicone samples showed high Shore C values (83.56 HC and 84.12 HC, respectively). Although these materials are typically classified as soft elastomers and are usually evaluated using the Shore A scale (47.5−57.5 HA for hydrophilic acrylic [46] and 20−90 HA for silicone [47]), the higher Shore C values observed in this study likely reflect specific material formulations or the presence of fillers that increase their stiffness. This highlights how a single measurement scale, while useful for direct comparison within a study, may not always reflect the traditional classifications found in literature, emphasizing the role of specific polymer formulations and testing conditions in determining mechanical properties. A comparison between literature and experimental data is shown in Table 1, and a histogram of the data is reported in Figure 8a. These observations motivate follow-up modulus-based mechanical testing (e.g., tensile testing, DMA, and/or nanoindentation), ideally under immersion conditions, to quantify deformation-relevant behavior more directly.

The experimental Shore C values for hydrophilic acrylic and silicone are not only higher than their theoretical normalized values but are also implausibly high for these materials. Conversely, the experimental PMMA value is significantly lower than its normalized Shore C value. These results underline the critical importance of using the correct Shore scale for each material to ensure accurate and reliable comparative analysis [48].

*In vivo*, the UV dose reaching an implanted IOL is substantially lower than external UV levels, owing to spectral filtering by the ocular media. As previously documented [29, 38], the cornea and crystalline lens together attenuate UV radiation considerably below 400 nm; this filtering is also age-dependent and varies with lens yellowing over time. The UV fluence and spectral content reaching intraocular structures therefore depend on patient-specific factors including geography, lifestyle, pupil size, and the use of protective eyewear.

In addition to UV radiation, other environmental and biochemical factors may contribute to long-term IOL degradation *in vivo*. These include oxidative species present in the aqueous humor, adsorption of proteins and lipids onto the

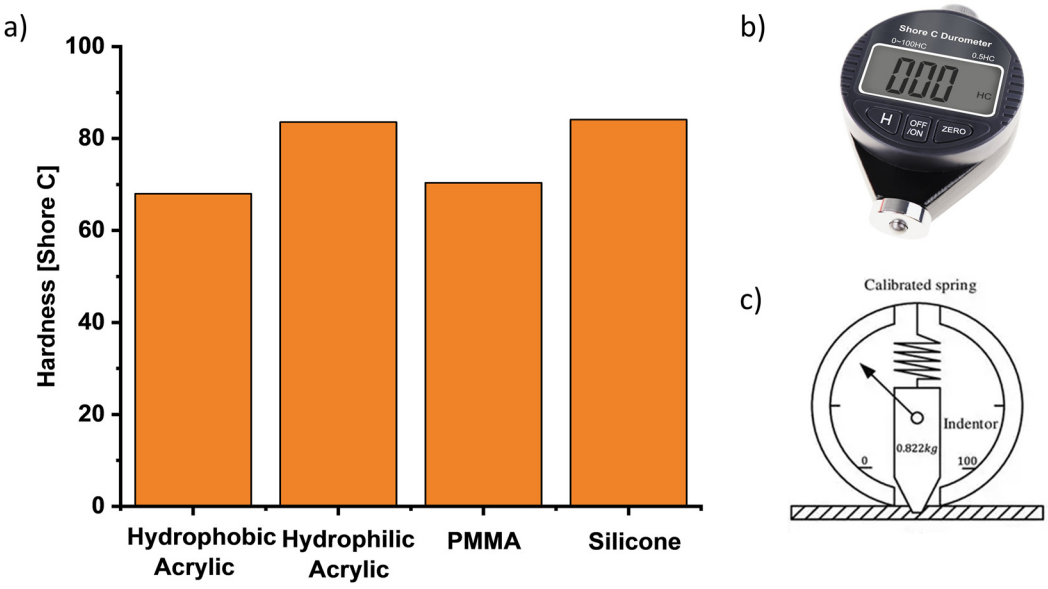


**Figure 8:** Shore C hardness assessment of UV-irradiated intraocular lens materials and measurement setup. (a) Shore C hardness values for hydrophobic acrylic, PMMA, hydrophilic acrylic, and silicone IOLs after UV irradiation. UV exposure induces stiffening of hydrophobic acrylic IOLs as reflected by increased hardness. (b) Photograph of the durometer employed for Shore C hardness measurements. (c) Schematic representation of the indentation principle.

lens surface, mechanical micro-stresses arising from capsular bag contraction and haptic interactions, and, in specific patient populations, exposure to ionizing radiation during radiotherapy. Additional environmental agents, including reactive vapors, elevated temperatures, high-intensity visible radiation, and reactive liquids, may further contribute to material degradation. The combined action of these factors with UV-driven photo-oxidative aging has not yet been characterized for hydrophobic acrylic IOLs and represents an important direction for future work. The present accelerated UV irradiation study in dry air should therefore be interpreted as an isolated probe of UV-driven degradation pathways rather than a complete model of clinical aging. Follow-up studies under physiological aqueous immersion and, ideally, under combined degradation conditions are recommended to better approximate the *in vivo* environment and assess potential synergistic effects on IOL optical and mechanical performance.

## 4 Conclusions

The multi-modal accelerated-UV characterization performed in this study shows that hydrophobic acrylic intraocular lenses (IOLs), widely used for their biocompatibility, low water uptake, and resistance to glistening formation, show measurable optical, chemical, surface, and mechanical modifications when exposed to prolonged UV irradiation. Overall, the combined dataset suggests that UV-driven aging can affect multiple material attributes that are relevant to long-term optical quality and handling-related properties, even when macroscopic transparency remains largely preserved.

The main results of this study can be summarized as follows:

(i) UV–Vis spectrophotometry showed a net decrease in transmittance in the UV region (up to 40 %) and in the short-wavelength visible range (10–20 %) after 25 h of irradiation, accompanied by an increase in absorbance consistent with the formation of additional absorbing centers within the polymer matrix.

(ii) ATR–FTIR spectroscopy confirmed the presence of UV-driven photochemical and photo-oxidative processes, indicating modifications of the acrylate backbone, including reduced aliphatic C–H stretching contributions and an enhanced carbonyl region, consistent with photo-oxidative processes such as chain scission and ester-linkage rearrangement; siloxane-related Si–O–Si features showed only minor changes, suggesting comparatively higher stability of the siloxane component under the present conditions.

(iii) Contact-angle measurements revealed a transient increase in apparent hydrophobicity, with peak times of approximately 3 h for both test liquids, with a more pronounced hydrophobic shift for the glucose solution (84°) than for distilled water (71°); this behavior

is consistent with competing surface reorganization and oxidation-driven processes.

(iv) Mechanical characterization showed a monotonic increase in Shore C hardness after prolonged UV exposure, reflecting UV-driven material stiffening. Shore C hardness increased from 63.0 to 73.1 after 25 h of UV exposure, indicating UV-induced stiffening compatible with additional cross-linking and increased network density.

Although indentation hardness is not a direct measure of elastic modulus, it provides a sensitive screening parameter for detecting early mechanical changes under controlled conditions.

Overall, these results show that hydrophobic acrylic IOLs can undergo measurable UV-induced evolution even when macroscopic transparency remains largely preserved. The concurrent emergence of additional absorbing centers, spectroscopic signatures of backbone modification, transient surface-wetting changes, and increased indentation hardness together provide convergent evidence for photochemical and photo-oxidative aging processes. From a functional perspective, the observed optical changes may be relevant to long-term optical quality, particularly with respect to contrast and stray-light mechanisms, while the surface and mechanical responses may affect handling-relevant properties and interfacial interactions. The present study has inherent limitations, including the use of dry-air irradiation rather than physiological aqueous solution, the characterization of a single IOL model, and the indirect nature of Shore C as a mechanical parameter, which directly motivate the following research directions.

Future work to support a more complete understanding of long-term IOL aging and its potential impact on optical performance and handling properties will include modulus-based mechanical testing (dynamic mechanical analysis, tensile testing, and nanoindentation under immersion), denser temporal sampling, and photostability experiments under physiologically representative aqueous conditions. Additional IOL models from different manufacturers will also be examined, and standard 0.9 % NaCl saline will be included among probe liquids to explicitly assess the role of ionic strength in the wetting response.

**Funding information:** The authors state no funding involved.

**Author contributions:** All authors have accepted responsibility for the entire content of this manuscript and approved its submission.

**Conflict of interest:** Alfio Torrisi, who is the co-author of this article, is a current Editorial Board member of *Open Physics*. This fact did not affect the peer-review process. The authors state no other conflict of interest.

**Data availability statement:** The datasets generated and/or analysed during the current study are available from the corresponding author on reasonable request.

## References

1. Luo C, Wang H, Chen X, Xu J, Yin H, Yao K. Recent advances of intraocular lens materials and surface modification in cataract surgery. Front Bioeng Biotechnol 2022;10:913383.
2. Tjia KF. The science behind hydrophobic acrylic lens materials. Cataract Refract Surg Today Eur 2011;34—6.
3. Kook D, Shajari M, Kohnen T. Hydrophobic acrylic intraocular lens. In: Encyclopedia of ophthalmology. Berlin, Heidelberg: Springer; 2018:901—2 pp.
4. Yildirim TM, Fang H, Schickhardt SK, Wang Q, Merz PR, Auffarth GU. Glistening formation in a new hydrophobic acrylic intraocular lens. BMC Ophthalmol 2020;20:186.
5. South East Eye Surgeon. The humble hydrophobic IOL; 2024. Available from: https://www.southeasteyesurgeon.co.uk/latest-updates-insights/2024/10/6/lh8y044yiqeoa3a8q5m0c0ifjoafh1.
6. Grzybowski A, Markeviciute A, Zemaitiene R. A narrative review of intraocular lens opacifications: update 2020. Ann Transl Med 2020;8:1546.
7. Torrisi A, Roszkowska A, Cutroneo M, Torrisi L. Irradiation of hydrophilic acrylic intraocular lenses by a 365 nm UV lamp. Phys Status Solidi A 2024;221:240097.
8. Tehrani M, Dick HB, Wolters B, Pakula T, Wolf E. Material properties of various intraocular lenses in an experimental study. Ophthalmologica 2004;218:57—63.
9. Wu KY, Khammar R, Sheikh H, Marchand M. Innovative polymeric biomaterials for intraocular lenses in cataract surgery. J Funct Biomater 2024;15:391.
10. McIntyre S, Werner L, Mamalis N. Hydrophobic acrylic IOLs: a primer. Cataract Refract Surg Today Eur 2011;39—44.
11. Pai HV, Pathan A, Kamath YS. A comparison of posterior capsular opacification after implantation of three different hydrophobic square edge intraocular lenses. Indian J Ophthalmol 2019;67:1424—7.
12. Wu Q, Li Y, Wu L, Wang CY. Hydrophobic versus hydrophilic acrylic intraocular lens on posterior capsule opacification: a meta-analysis. Int J Ophthalmol 2022;15:990—6.
13. Özyol P, Özyol E, Karel F. Biocompatibility of intraocular lenses. Turk J Ophthalmol 2017;47:221—5.
14. Scolaro C, Torrisi L, Cutroneo M, Velardi L. Surface analysis of ion-implanted PMMA for intraocular lens applications. J Phys Conf Ser 2014;508:012030.
15. Lee Y, Kim JS, Kim BG, Hwang JH, Kang MJ, Kee JH. Comparison of the incidence of Nd:YAG laser capsulotomy based on the type of intraocular lens. Medicina 2023;59:2173.
16. Montrimas A, Rinkevičiūtė J, Žemaitienė R. Posterior capsule opacification treatment using Nd:YAG laser capsulotomy: 36 months retrospective analysis. BMC Ophthalmol 2025;25:197.
17. Eliasson B, Packer M, Mamalis N, Werner L. Surface properties of commercially available hydrophobic acrylic intraocular lenses. J Cataract Refract Surg 2016;42:406—12.

18. Kim TH, Song KC. Effect of hydrophobic acrylic monomers with different alkyl side chain lengths on reducing the glistening of hydrophobic acrylic intraocular lens materials. ChemistrySelect 2024;9:e202403573.
19. Tan X, Zhan J, Zhu Y, Cao J, Wang L, Liu S, et al. Improvement of uveal and capsular biocompatibility of hydrophobic acrylic intraocular lens by surface grafting with 2-methacryloyloxyethyl phosphorylcholine methacrylic acid copolymer. Sci Rep 2017;7:40462.
20. Torrisi L. Ion irradiation of polymethylmetacrylate (PMMA). Radiat Eff Defect Solid 1998;145:285—96.
21. Torrisi L, Roszkowska AM, Silipigni L, Cutroneo M, Torrisi A. Effects of 365 nm UV lamp irradiation of polymethylmethacrylate (PMMA). Radiat Eff Defect Solid 2024;179:264—74.
22. Torrisi A, Roszkowska A, Cutroneo M, Silipigni L, Torrisi L. Spectroscopic analysis of silicone intraocular lenses by optical transmission measurements and FTIR. Int Polym Process 2025;39:490—6.
23. Chen Y, Kearns VR, Zhou L, Sandinha T, Lam WC, Steel DH, et al. Silicone oil in vitreoretinal surgery: indications, complications, new developments and alternative long-term tamponade agents. Acta Ophthalmol 2021;99:240—50.
24. Zare M, Bigham A, Zare M, Luo H, Ghomi ER, Ramakrishna S. pHEMA: an overview for biomedical applications. Int J Mol Sci 2021;22:6376.
25. Schartmüller D, Lisy M, Mahnert N, Schranz M, Danzinger V, Schwarzenbacher L, et al. Rotational stability and refractive outcomes of a new hydrophobic acrylic toric intraocular lens. Eye Vis 2024;11:25.
26. Negishi K, Masui S, Torii H, Nishi Y, Tsubota K. Refractive stability of a new single-piece hydrophobic acrylic intraocular lens and corneal wound repair after implantation using a new automated intraocular lens delivery system. PLoS One 2020;15:e0238366.
27. Torrisi A, Cutroneo M, Torrisi L, Lavalle S, Forzina A, Pegreffi F. Unveiling the potential of vitamin D3 orodispersible films: a comprehensive FTIR and UV—Vis spectroscopic study. Molecules 2024;29:3762.
28. Vacalebre M, Frison R, Corsaro C, Neri F, Santoro A, Conoci S, et al. Current state of the art and next generation of materials for a customized intraocular lens according to a patient-specific eye power. Polymers (Basel) 2023;15:1590.
29. Boettner EA, Wolter JR. Transmission of the ocular media. Investig Ophthalmol Vis Sci 1962;1:776—83.
30. Yang S, Makker H, Christ RF. Accelerated ultraviolet aging of intraocular lens optic materials: a 50-year simulation. J Cataract Refract Surg 1997;23:940—7.
31. Torrisi A, Roszkowska A, Cutroneo M, Torrisi L. Irradiation of PMMA intraocular lenses by a 365 nm UV lamp. Int Polym Process 2024;39:490—6.
32. MacFarlane ER, Donaldson PJ, Grey AC. UV light and the ocular lens: a review of exposure models and biomolecular changes. Front Ophthalmol 2024;4:1414483.
33. Troisi M, Rossi G, Bianchi L, Costigliola C, Semeraro F, Romano V. Experimental investigation of the causes of intraocular lens opacification. Investig Ophthalmol Vis Sci 2025;66:2804339 (ARVO Annual Meeting Abstracts).
34. Hanita Lenses. Aspheric HP; 2025. Available from: https://www.hanitalenses.com/intraocular-implants/monofocal/aspheric-hp/.
35. ASTM International. Standard practice for operating fluorescent ultraviolet (UV) lamp apparatus for exposure of nonmetallic materials, ASTM G154-16. ASTM International; 2025. Available from: https://img.antpedia.com/standard/files/pdfs_ora/20200926/ASTM%20G154-16.pdf.
36. Fisher Scientific. UVL-56 handheld UV lamp; 2025. Available from: https://www.fishersci.co.uk/shop/products/uvl-56-handheld-uv-lamp/11738221.
37. ASTM International. Standard test method for rubber property-durometer hardness, ASTM D2240-21. ASTM International; 2021. Available from: https://www.plantech.com/wp-content/uploads/2017/05/ASTM-D2240-Durometer-Hardness.pdf.
38. Hayashi K, Hirata A, Yoshida M, Yoshimura K, Hayashi H. Long-term effect of surface light scattering and glistenings of intraocular lenses on visual function. Am J Ophthalmol 2012;154:240—51.
39. Sharma A, Pande PP. Synthesis of poly(n-butyl acrylate) with TEMPO by nitroxide mediated polymerization method. Polym Polym Compos 2021;29:S895—02.
40. Xu X, Tang JM, Han YM, Wang W, Chen H, Lin QK. Surface PEGylation of intraocular lens for PCO prevention: an in vivo evaluation. J Biomater Appl 2016;31:68—76.
41. Lin TY, Pfeiffer TT, Lillehoj PB. Stability of UV/ozone-treated thermoplastics under different storage conditions for microfluidic analytical devices. RSC Adv 2017;59:37374—9.
42. Huang Z, Wang H. Turning danger into opportunity: ultraviolet (UV) irradiation-surface reconstruction effect of hydrophilic plastics and its application in plastic flotation separation. J Environ Chem Eng 2023;11:110659.
43. Kumar M, Arun S, Upadhyaya P, Pugazhenthi G. Properties of PMMA/clay nanocomposites prepared using various compatibilizers. Int J Mech Mater Eng 2023;10:7.
44. Eyewiki. Comparison of IOL materials; 2024. Available from: https://eyewiki.org/Comparison_of_IOL_Materials.
45. Hapco Inc. Comparison of IOL materials. Hardness conversion chart; 2025. Available from: https://hapcoincorporated.com/resources/hardness-chart/.
46. Aki D, Rad ME, Şenel EC, Onceyiz MC, Gokmenoglu MC, Dut L, et al. Fine-tuning equilibrium water content and mechanical properties of acrylic-based copolymers for intraocular lens applications. Biomed Mater 2025;20:045026.
47. Legenday. Understanding the shore hardness of silicone rubber; 2025. Available from: https://legenday.com.cn/understanding-the-shore-hardness-of-silicone-rubber/.
48. Imperial Rubber Products Inc. How to determine the hardness of rubber rollers; 2012. Available from: https://www.sme.in/imperialrubber/determining_the_hardness_of_roller_rubber.html.